J Mater Sci (2010) 45:2708–2714
DOI 10.1007/s10853-010-4256-3

The influence of the lateral filament texture on the compressive properties of PpPTA aramid filaments

Alwin Knijnenberg · Ben Koenders · Bert Gebben · Enno Klop · Robert J. Young · Sybrand van der Zwaag

Received: 8 October 2009 / Accepted: 20 January 2010 / Published online: 4 February 2010

Abstract A series of PpPTA aramid fibres with various degree of lateral orientation ranging from their usual radial-oriented lateral texture to a full random lateral texture were prepared by employing a series of different coagulating media in the fibre spinning process. The resulting variation in lateral texture did not lead to differences in linear tensile properties or crystallite dimensions. Raman spectroscopy measurements on embedded axially compressed filaments showed that the stresses for kink band initiation and propagation were independent of the degree of lateral texture. The kink band morphology and the final kink band density upon further straining were found to correlate with the shear modulus derived from combined mechanical and XRD data.

Introduction

Poly(*para*-phenylene terephthalamide), PpPTA, aramid fibres are a special class of high performance fibres which combine high specific strength and specific stiffness with great thermal stability and good solvent resistivity [1, 2]. Their properties are determined by a combination of a highly aromatic polymer backbone structure with an internal microstructure comprising a high degree of orientation in the axial direction and some orientation in the lateral packing direction [3]. Northolt has presented a model to link the mechanical properties of such fibres in the axial direction to their physical microstructure [4–6]. To this aim the relevant structure of a filament was represented as a linear end-to-end arrangement of crystallites oriented at a small angle ϕ with respect to the filament axis. The two principal deformation mechanisms in this model are elastic chain stretching and crystallite orientation. From this model it follows that the elastic modulus of aramid fibres is limited intrinsically by the chain modulus. The actual modulus, however, is largely determined by the average crystallite disorientation angle ϕ. Moreover, the molecular order within a filament is likely to reflect the average molecular order in the PPTA polymer–sulphuric acid mixture, the spin dope, from which the fibres are spun, which was confirmed by a quantitative study by Picken et al. [7].

Despite quite a good understanding of the structure–property relationships and ultimate properties of aramid fibre under tension, axial compressive failure behaviour is still relatively poorly understood. Although great effort has been made to improve compressive properties—e.g. by introducing crosslinks between the polymer chains [8–10] the nature of the exact failure mechanism and the defining microstructural parameters are still not known in detail. At present, most attempts for improving fibre compressive properties are primarily aimed at increasing lateral cohesive forces between polymer chains, either by changing the heat treatment or via chemical crosslinking. However, the microscopic lateral internal filament microstructure may also play an important role in governing compressive properties. So far, the role of the aramid filament

A. Knijnenberg · S. van der Zwaag (✉)
Fundamentals of Advanced Materials Group, Faculty of Aerospace Engineering, Delft University of Technology, Kluyverweg 1, 2629 HS Delft, The Netherlands
e-mail: S.vanderZwaag@tudelft.nl

B. Koenders · B. Gebben · E. Klop
Research Institute, Teijin Aramid B.V., P.O. Box 9300, 6800 SB Arnhem, The Netherlands

R. J. Young
Materials Science Centre, School of Materials, The University of Manchester, Manchester M1 7HS, UK

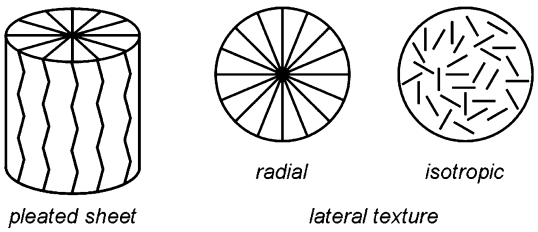

Fig. 1 Microstructural features in aramid fibres; the pleated sheet (*left*) and radially oriented texture (*middle*). An isotropic lateral texture (*right*) can be obtained when using alternative coagulants

microstructure in relation to its compressive strength has not been taken into account. For aramid fibres at least two distinct microstructural features can be identified, see Fig. 1. The first one is the so-called pleated sheet structure, a periodic fluctuation in the axial orientation of the hydrogen-bonded planes [11]. The alternating planar surfaces with their misorientation angles of 5°–7° with respect to the fibre axis have a spacing of around 250–400 nm and these characteristics are virtually independent of spinning conditions. Pleated sheet-like microstructures have been observed in fibres based on lyotropic [12–15] as well as thermotropic [16, 17] liquid crystalline polymers and even in fibres based on supramolecular quasi-linear platinum compounds [18]. The physical origin of the pleated sheet has, however, still not been clarified but it is known that it plays an important role in fibre properties, e.g. it affects the average molecular orientation and directly influences the fibre modulus. A second microstructure commonly found in commercial aramid yarns is the radial texture [15, 19, 25]. Usually, crystallites in aramid fibres are oriented in such a way that the hydrogen bonds between neighbouring chains in the PpPTA crystal unit cell are directed perpendicular to the fibre skin, leading to a so-called radial texture. The degree of radial texture depends on several factors, such as the polymer concentration in the polymer–sulphuric acid mixtures from which the fibres are spun, and the coagulant. Using less polar coagulants it can be tuned from the regular well-developed radial texture in all commercial water spun PpPTA aramid fibres to a full laterally isotropic state even for high polymer concentrations in the polymer–sulphuric acid mixtures [11, 20].

It is imaginable that changing the degree of lateral orientation of the hydrogen-bonded planes will result in a change of the overall lateral cohesion within the aramid fibre and hence in its compressive strength. In order to gain more insight into the mechanisms influencing compressive properties, we changed the fibre microstructure by employing different coagulating media. We obtained a series of aramid fibres with various lateral textures ranging from quasi isotropic to a radially oriented structure, but with comparable axial mechanical properties. In this paper we describe the characterization of this series of aramid fibres, focusing on the influence of the lateral texture on the compressive failure mechanisms.

Experimental

Materials

A collection of 5 sets of fibres was spun using the standard dry-jet wet spinning technique using a regular 19.7 PpPTA wt%–sulphuric acid mixture and the usual parameter settings. The spinning process was modified and turned into a two-step coagulation process. The coagulation conditions were varied by changing the composition of the first coagulation bath using different types or combinations of types of fluids as listed in Table 1. Residence times in the first coagulation bath were about 5 s. The bath compositions were based on earlier research and are listed in Table 1 [20]. The second coagulation bath contained water and the residence time in this bath was about 10 s prior to winding the fibres on a bobbin. Subsequently, the fibres on the bobbin were washed for several hours to assure complete removal of the sulphuric acid. A stable spinning process yielding smooth filaments with a shiny appearance was obtained for the 5 types of coagulation media employed and the correct settings of bath temperatures and line tensions.

Physical characterization

A Jena interference microscope was used to determine the degree of lateral texture using polarised monochromatic

Table 1 Coagulation media and corresponding physical properties (taken from the literature) and mechanical properties of aramid fibres with variable lateral textures

Yarn	Coagulant	ε_r (–)	δ (cal$^{1/2}$ cm$^{3/2}$)	n_r	n_l	Δn_{lat}	λ110 (nm)	λ200 (nm)
PpPTA-R1	Water	87	23.5	1.646	1.606	0.040	60	49
PpPTA-R2	50/50 Ethanol/water	53	18.2	1.650	1.610	0.040	46	47
PpPTA-R3	67/33 Ethanol/water	42	16.4	1.636	1.618	0.018	53	48
PpPTA-R4	Methanol	33	14.28	1.642	1.624	0.018	58	46
PpPTA-R5	75/25 Ethanol/dichloromethane	19	12.2	1.627	1.625	0.002	57	46

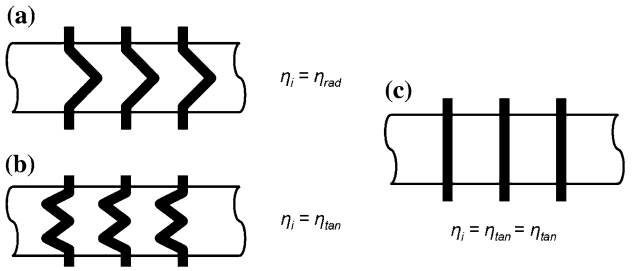

Fig. 2 Schematic representation of the interference patterns required for the determination of the radial (**a**) and tangential (**b**) refractive index for a fibre with a well-developed radial texture. For a fibre with a randomly oriented radial texture, refractive indices will be similar and an interference pattern as in **c** will appear

light ($\lambda = 546$ nm), with the polarization direction perpendicular to the filament axis. Such an experimental set-up can be used to determine the refractive indices in both the radial (n_{rad}) and tangential (n_{tan}) directions. The difference between n_{rad} and n_{tan} is a direct measure for the degree of radial orientation and is referred to as Δn_{lat}. The indices can be determined by adjusting the refractive index of the immersion fluid until the required interference patterns belonging to either n_{rad} or n_{tan} (see Fig. 2) is observed. To avoid mixing of immersion fluids, every sample was freshly prepared with a suitable Cargill refractive index fluid (series A and B). The immersion fluids available covered a range of refractive indices from 1.460 to 1.700 with intervals of 0.002. The patterns as shown schematically in Fig. 2 are representative for filaments with a well-developed radial texture. The lower the degree of radial orientation the smaller the amplitude of the V- and W-shaped patterns. The interference pattern for a filament with a randomly oriented lateral structure will approach straight continuous vertical lines, when using an immersion fluid of the appropriate refractive index.

It is noted that this technique for measuring both lateral refractive indices can only be employed if the two crystal refractive indices n_α and n_β are unequal. Another prerequisite for accurate determination of the degree of lateral texture is the uniformity of the crystallite orientation parallel to the fibre axis over the filament cross-section which can be verified by measuring $n^{\parallel}$ and employing light polarised parallel to the filament axis. The linear density of the fibres was kept relatively low in order to avoid strong skin–core effects with accompanying differences in crystallite orientation and other spinning defects related to large diameter fibre spinning.

X-ray diffraction was used to determine the crystal unit cell parameters and the apparent lateral crystal size. The XRD measurements were carried out on a Bruker D8 diffractometer in $\theta/2\theta$ geometry, equipped with parallel beam optics. The optics consist of a primary 60 mm Göbel focussing mirror (a parabolic Ni/C multilayer device) providing Cu Kα radiation, and 0.12° Soller slits. The diffractometer is equipped with scintillation detector and autochanger.

Mechanical characterization

The linear tensile properties were determined on an Instron 5543 tensile tester. For each fibre 10 filaments with a gauge length of 100 mm were tested at a speed of 10 mm min^{-1}. Experiments were performed under standard laboratory conditions of 21 °C and 65% relative humidity. The compressive properties of axially compressed embedded single filaments were determined by kink band initiation and local stresses were probed by means of Raman spectroscopy [21, 22]. Details for the experimental procedure are published elsewhere [23].

Raman spectroscopy

Raman spectra were obtained using a Renishaw 1000 spectrometer equipped with a 30 mW HeNe laser (wavelength 633 nm). A 50× objective lens was used in the spectrometer microscope which focussed the laser beam to a spot of around 2 μm. The laser beam intensity at the sample was kept to <1 mW.

Results and discussion

Lateral texture measurements

The degree of radial orientation within the single filaments was determined by interference microscopy and examples of such images are shown in Fig. 3a, b for a PpPTA-R2 filament, coagulated in a 50/50 ethanol/water mixture. The micrographs show well-defined striping patterns without any defects indicating that the filaments are of good quality. The characteristic V- and W-shaped patterns as schematically shown in Fig. 2 can be clearly distinguished and

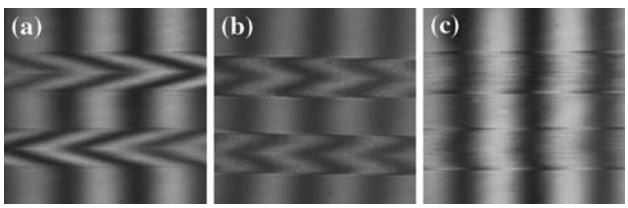

Fig. 3 Typical examples for the interference patterns for the determination of n_{rad} and n_{tan}. The patterns **a** and **b** with n_{rad} and n_{tan} equal to 1.650 and 1.610, respectively, were measured for PpPTA-R2 and indicate a strong radial-oriented texture ($\Delta n_{lat} = 0.040$). Pattern **c** is obtained on PpPTA-R5 and yielded n_{rad} and n_{tan} equal to 1.627 and 1.625, respectively, which corresponds to an isotropic lateral ordering ($\Delta n_{lat} \cong 0.002$)

correspond to radial and lateral refractive indices. These values of 1.650 and 1.610, respectively, result in a Δn_{lat} equal to 0.040 which indicates a fully developed radially oriented texture. Figure 3c shows the interference pattern found for a PpPTA-R5 single filament, where refractive indices in both radial direction (n_{rad}) and tangential (n_{tan}) direction are found to be almost identical and equal to 1.627 and 1.625, respectively. The resulting measure for the degree of radial texture Δn_{lat} for this fibre, coagulated in a mixture of 75% ethanol and 25% dichloromethane, is equal to 0.002 which is indicative for a highly isotropic lateral ordering.

The refractive index values for the fibres in both radial and tangential directions as measured by interference microscopy are listed in Table 1, which also contains the results of the crystallite size determination. The values for Δn_{lat} which follows directly from these two indices show that the series of fibres cover the full range of lateral textures, from a well-developed radial texture ($\Delta n_{lat} = 0.040$) to a randomly oriented lateral texture ($\Delta n_{lat} = 0.002$).

These results show that the composition of the coagulation bath has a large influence on the degree of radial orientation in the fibre. Considering the limited accuracy of the Δn_{lat} determination, these results are consistent with data reported by van der Zwaag and co-workers [11, 20]. They found a linear relation between the solubility parameter and the lateral birefringence Δn_{lat}, also indicated in Fig. 4a by the solid line. The exact physical process responsible for the formation of the radial texture during the coagulation remains, however, to be identified.

There seems to be no relationship between the apparent crystallite sizes $\lambda 110$ and $\lambda 200$, listed in Table 1, and the degree of lateral texture. This suggests that the molecular and microscopic order within the aramid filaments are independent of each other and can be controlled independently.

Tensile mechanical properties

All fibres had a smooth shiny surface and a regular optical appearance that is generally found for experimental PpPTA fibres. The linear tensile data as presented in Table 2 show that axial fibre properties do not vary much between the five grades, notwithstanding significant changes in coagulation conditions. Fibre tenacities as well as tensile moduli are all at the level expected and the observed scatter is the result of small variations in line tension during spinning in the experimental setup. Furthermore, for all grades the shape of the stress–strain curve was identical to those for regular as-spun and air-dried aramid fibres.

In addition to apparent crystallite sizes, the average orientation parameter was also determined by XRD and is listed in Table 2. From this orientation parameter and the fibre modulus data, the shear modulus can be deduced using the Northolt model [5, 6]. In this model the fibre modulus E can be described in terms of the chain modulus e_c, the orientation parameter $\langle \sin^2 \Phi \rangle$ and the shear modulus g, in a manner given by Eq. 1:

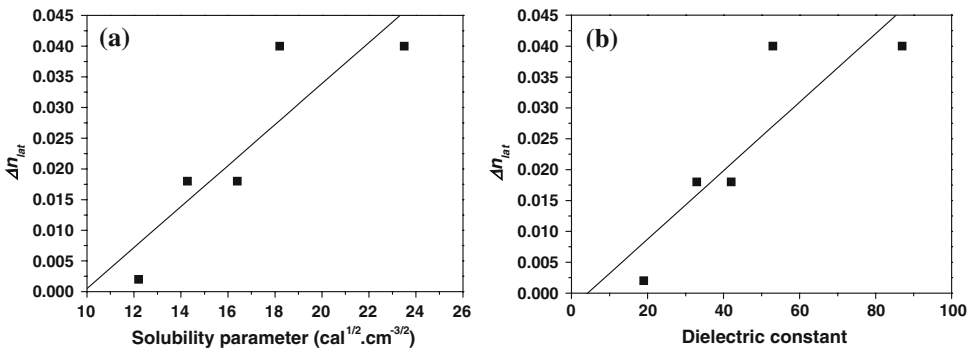

Fig. 4 The relations between the solubility parameter (**a**) and the dielectric constant (**b**) of the coagulant and resulting degrees of radial orientation within the corresponding fibres. The *solid line* indicates the linear relation between coagulant properties and degree of radial orientation

Table 2 Physical and mechanical properties of fibres with various lateral textures

Yarn	LD (dtex)	Tenacity (mN tex^{-1})	Modulus (GPa)	$\langle \sin^2 \Phi \rangle$	Shear modulus (GPa)
PpPTA-R1	2.37	2001 ± 152	90	0.020	1.44
PpPTA-R2	1.95	1856 ± 143	89	0.017	1.20
PpPTA-R3	2.11	2041 ± 123	113	0.021	2.24
PpPTA-R4	1.88	1793 ± 180	96	0.014	1.12
PpPTA-R5	1.68	1987 ± 160	111	0.024	2.48

$$\frac{1}{E} = \frac{1}{e_c} + \frac{\langle \sin^2 \Phi \rangle_E}{2g} \quad (1)$$

The values found for g range from 1.20 to 2.48 GPa which is in line with a typical value of 1.8 GPa found for aramid fibres [6]. Based on the data from this set of experiments, it appears that there is no direct relationship between the fibre lateral texture and the shear modulus.

Compressive failure behaviour

To gain more insight in the influence of the lateral texture on the compressive failure behaviour, single filaments were embedded in a cold curing epoxy and compressed axially. Two types of kink band morphologies and kink band behaviour as a function of the strain level could be distinguished. The corresponding micrographs showing the development of kink bands in a PpPTA-R2 and a PpPTA-R3 filament are shown in Fig. 5.

For both types of fibres single-tilted kink bands are the dominating morphology at strains just above the critical strain for kink band initiation. Upon further axial compression the behaviour of the filaments starts to deviate resulting either in the formation of new extended kink bands or enlargement of the deformation in existing kink bands. This difference leads to significant differences in the final kink band density for filament PpPTA-R2 (high kink band density) and filament PpPTA-R3 (low kink band density). A similar behaviour of few but thick kink bands at high compressive strains as recorded for PpPTA-R3 was observed for PpPTA-R5, while the filaments PpPTA-R1 and PpPTA-R4 showed behaviour akin to that of PpPTA-R2. It is interesting to note that the difference in kink band density development upon further compressive straining does not correlate with the degree of lateral texture, but does correlate with the shear modulus as derived from the XRD data (Table 2). Samples with a low shear modulus PpPTA-R1, -R2 and -R4 have thinner kink bands which develop more uniformly in between existing kink bands, while sample with a high shear modulus (PpPTA-R3 and -R5) show a strong localisation of the deformation in kink bands that form initially and a slower increase in kink band density upon further straining.

The development of compressive stress as a function of applied axial strain was monitored using Raman spectroscopy. Raman spectra were recorded without any difficulties resulting in a collection of well-defined peaks at positions similar to those found in standard aramid yarns. The shift of the Raman active 1610 cm^{-1} band as a function of compressive strain is shown in Fig. 6. The slope of the Raman curve as a function of strain could be linearly approximated and was found to be equal to 2.06 ± 0.21 cm^{-1} per %, before reaching the maximum shift at 1.08 ± 0.07 cm^{-1}. The corresponding maximum attainable compressive stress therefore is 0.27 ± 0.02 GPa using the universal calibration factor for aramids of 4 cm^{-1} per GPa [24, 25]. The stress relaxation as was measured by the average decrease of the Raman wave number on the 1.5–2.5% strain interval compared to the maximum measured shift is found to be 0.32 ± 0.09 cm^{-1}. The equilibrium stress that was finally reached is equal to 0.19 ± 0.02 GPa.

Figure 6 is a representative example for all fibres measured within this research. The key parameters as obtained by Raman spectroscopy are summarised in Table 3. The maximum compressive stress level as measured with the maximum Raman shift is found to be constant within experimental error and on average around 0.30 GPa.

The data in Fig. 7a suggest that the critical compressive strain ε_c has only a weak dependence upon the degree of

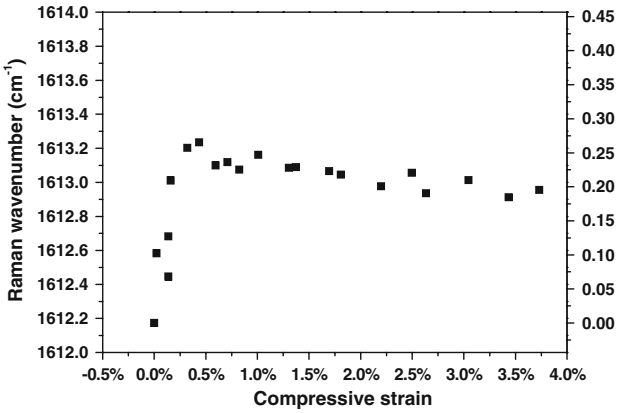

Fig. 6 Position of the Raman 1610 cm^{-1} peak as a function of strain for a single PpPTA-R2 filament loaded in pure axial compression

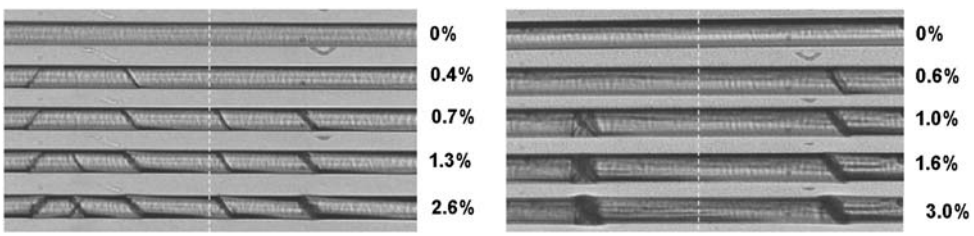

Fig. 5 Formation of kink bands in a PpPTA-R2 (*left*) and a PpPTA-R3 (*right*) fibre loaded in pure axial compression. The *dashed lines* indicate the point where the local stress was probed (focus of the Raman laser beam)

Table 3 Key parameters as directly derived from the Raman band shift curves (local stress levels were calculated from the total Raman shift with respect to the zero strain reference level and a correlation factor of 4 cm^{-1} per GPa [25])

Yarn	$\Delta\nu/\varepsilon$ (cm^{-1}/%)	σ_c (GPa)	$\sigma_{plateau}$ (GPa)
PpPTA-R1	3.26 ± 0.13	0.30 ± 0.04	0.21 ± 0.02
PpPTA-R2	2.06 ± 0.21	0.27 ± 0.02	0.19 ± 0.02
PpPTA-R3	2.23 ± 0.17	0.28 ± 0.03	0.20 ± 0.02
PpPTA-R4	3.04 ± 0.23	0.29 ± 0.05	0.25 ± 0.06
PpPTA-R5	3.05 ± 0.15	0.33 ± 0.04	0.22 ± 0.03

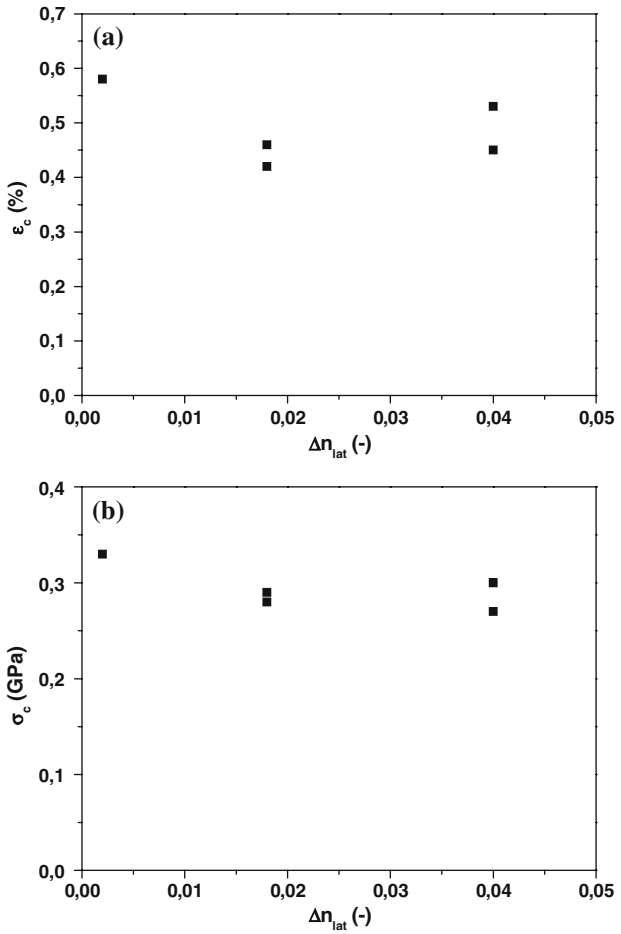

Fig. 7 **a** Critical compressive strain ε_c and **b** critical compressive strength σ_c of single filaments as a function of the degree of lateral orientation Δn_{lat}

lateral texture. Furthermore, constant compressive strengths as shown in Fig. 7b, suggest that the presence or absence of a radial texture does neither influence this strength. Similar conclusions can be drawn for values found for the rate of band shift $\Delta\nu/\varepsilon$ and for the plateau stress during kink band formation $\sigma_{plateau}$.

In summary, the results of the Raman measurements revealed that the degree of radial orientation in the fibre at best only has a small influence on the compressive failure behaviour. This conclusion is in agreement with the compressive failure mechanism as proposed by Lacks [25]. He suggested that the elastic buckling of the crystallites was the determining factor for the compressive strength of the fibre. The current results would be in line with such an explanation, confirmed by the fact that all fibres have similar apparent crystallite sizes as measured by XRD [26].

The results obtained here shed a new light on the relationship between the compressive strength and the shear modulus. In early work a strong correlation was demonstrated between the compressive strength of various high performance fibres and their shear or torsion modulus [5, 27]. However, within the current data set of polymer fibres of the same chemical structure, this correlation was not observed. All PpPTA fibres have essentially the same critical stress for the onset of kink band formation, irrespective of their shear modulus or degree of lateral texture, but the two kink band morphologies observed were found to correlate well to the two levels of shear moduli derived from combined mechanical and XRD data.

Conclusions

The degree of radial orientation in PpPTA aramid fibre seems to have a minor effect on the onset of compressive failure, i.e. the formation of the first kink band, in the case of axial loading of embedded single filaments. Upon further straining of the filaments two types of kink band morphologies were observed, which did not correlate to the degree of lateral texture but rather to the shear modulus derived from combined mechanical and XRD data. A high shear modulus was found to correspond to the concentration of the further compressive deformation in existing kink bands rather than in the formation of new kink bands found in the case of a lower shear modulus.

References

1. Hearle J (2001) High-performance fibres. Woodhead Publishing Ltd, Cambridge
2. Cheng SZD, Li F, Li CY, McCreight KW, Yoon Y, Harris FW (2000) In: Salem DR (ed) Structure formation in polymeric fibers. Hanser, Munich, p 247
3. van der Zwaag S (2009) In: Eichhorn S, Hearle JWS, Jaffe M, Kikutani T (eds) Handbook of textile fibre structure, vol 1: Fundamentals and manufactured polymer fibres. Woodhead Publishing Ltd, Oxford, pp 394–412
4. Northolt MG (1980) Polymer 21:1199
5. Northolt MG, Baltussen JJM, Schaffers-Korff B (1995) Polymer 36:3485
6. Northolt MG, den Decker P, Picken SJ, Baltussen JJM, Schlatmann R (2005) Adv Polym Sci 178:1

7. Picken SJ, van der Zwaag S, Northolt MG (1992) Polymer 33:2998
8. Knijnenberg A, Bos J, Dingemans TJ (2010) Polymer (accepted)
9. Knijnenberg A (2009) Compressive failure behaviour of novel aramid fibres. PhD thesis, Delft University of Technology
10. Markoski LJ, Walker KA, Deeter GA, Spilman GE, Martin DC, Moore JS (1993) Chem Mater 5:248
11. Northolt MG, Sikkema DJ (1991) Adv Polym Sci 98:115
12. Avakian P, Blume, RC, Gierke TD, Yang HH (1980) Polym Prepr (Am Chem Soc, Div Polym Chem) 21:8
13. Dobb MG, Johnson DJ, Saville BP (1977) J Polym Sci, Part B: Polym Phys 15:2201
14. Dobb MG, Johnson DJ, Saville BP (1977) J Polym Sci Polym Symp 58:237
15. Hagege R, Jarrin M, Sotton M (1979) J Microsc 115:65
16. Donald AM, Viney C, Windle AH (1983) Polymer 24:155
17. Viney C, Donald AM, Windle AH (1983) J Mater Sci 18:1136. doi:10.1007/BF00551982
18. Fontana M, Caseri W, Smith P (2006) Platinum Metals Rev 50:112
19. Warner SB (1983) Macromolecules 16:1546
20. van der Zwaag S, Koenders B, Maatman H, Schenkels F (1987) Internal Report Akzo Research Laboratories, Arnhem, the Netherlands
21. Sinclair D (1950) J Appl Phys 21:380
22. van der Zwaag S, Northolt MG, Young RJ, Robinson IM, Galiotis C, Batchelder DN (1987) Polym Commun 28:276
23. Knijnenberg A, Young RJ, van der Zwaag S (2010) J Mater Sci (submitted)
24. Young RJ (1995) J Text Inst 86:360
25. Lacks DJ (1996) J Mater Sci 31:5885. doi:10.1007/BF01152137
26. Riekel C, Cedola A, Heidelbach F, Wagner K (1997) Macromolecules 30:1033
27. DeTeresa SJ, Porter RS, Farris RJ (1988) J Mater Sci 23:1886. doi:10.1007/BF01115735